JACS
JOURNAL OF THE AMERICAN CHEMICAL SOCIETY
Article
pubs.acs.org/JACS

Chiral Ceramic Nanoparticles and Peptide Catalysis

Shuang Jiang,[†,∥,Δ,⊥,¶] Mahshid Chekini,[†,∥] Zhi-Bei Qu,[†,∥] Yichun Wang,[†,∥,§] Aydan Yeltik,[∥,▼] Yuangang Liu,[†,▽] Alex Kotlyar,[†,∥] Tianyong Zhang,[Δ,⊥,¶] Bin Li,[Δ,⊥,¶] Hilmi Volkan Demir,[▼,◆] and Nicholas A. Kotov*[,†,∥,#,‡]

[†]Department of Chemical Engineering, [∥]Biointerfaces Institute, [#]Department of Materials Science and Engineering, [‡]Department of Biomedical Engineering, and [§]Department of Mechanical Engineering, University of Michigan, Ann Arbor, Michigan 48109, United States

[Δ]School of Chemical Engineering and Technology, Tianjin Key Laboratory of Applied Catalysis Science and Technology, Tianjin University, Tianjin 300354, China

[⊥]Collaborative Innovation Center of Chemical Science and Engineering (Tianjin), Tianjin 300354, China

[¶]Tianjin Engineering Research Center of Functional Fine Chemicals, Tianjin 300354, China

[▼]Department of Electrical and Electronics Engineering, Department of Physics, UNAM, Bilkent University, 06800 Ankara, Turkey

[◆]School of Electrical and Electronic Engineering, School of Physical and Mathematical Sciences, LUMINOUS! Center of Excellence for Semiconductor Lighting and Displays, Nanyang Technological University, 639798 Singapore

[▽]College of Chemical Engineering, Huaqiao University, Xiamen 361021, China

Supporting Information

ABSTRACT: The chirality of nanoparticles (NPs) and their assemblies has been investigated predominantly for noble metals and II−VI semiconductors. However, ceramic NPs represent the majority of nanoscale materials in nature. The robustness and other innate properties of ceramics offer technological opportunities in catalysis, biomedical sciences, and optics. Here we report the preparation of chiral ceramic NPs, as represented by tungsten oxide hydrate, $WO_{3-x}\cdot H_2O$, dispersed in ethanol. The chirality of the metal oxide core, with an average size of ca. 1.6 nm, is imparted by proline (Pro) and aspartic acid (Asp) ligands via bio-to-nano chirality transfer. The amino acids are attached to the NP surface through C−O−W linkages formed from dissociated carboxyl groups and through amino groups weakly coordinated to the NP surface. Surprisingly, the dominant circular dichroism bands for NPs coated by Pro and Asp are different despite the similarity in the geometry of the NPs; they are positioned at 400−700 nm and 500−1100 nm for Pro- and Asp-modified NPs, respectively. The differences in the spectral positions of the main chiroptical band for the two types of NPs are associated with the molecular binding of the two amino acids to the NP surface; Asp has one additional C−O−W linkage compared to Pro, resulting in stronger distortion of the inorganic crystal lattice and greater intensity of CD bands associated with the chirality of the inorganic core. The chirality of $WO_{3-x}\cdot H_2O$ atomic structure is confirmed by atomistic molecular dynamics simulations. The proximity of the amino acids to the mineral surface is associated with the catalytic abilities of $WO_{3-x}\cdot H_2O$ NPs. We found that NPs facilitate formation of peptide bonds, leading to Asp-Asp and Asp-Pro dipeptides. The chiroptical activity, chemical reactivity, and biocompatibility of tungsten oxide create a unique combination of properties relevant to chiral optics, chemical technologies, and biomedicine.

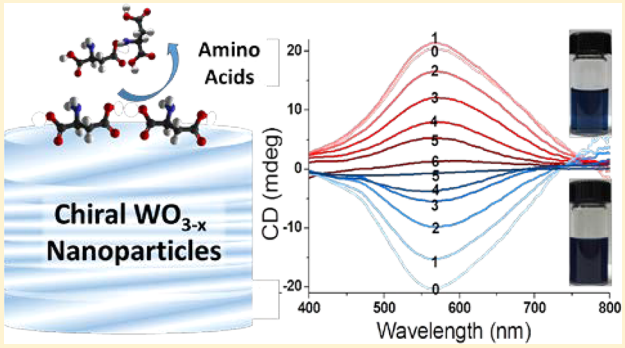

INTRODUCTION

Chiral inorganic nanostructures represent one of the fastest growing areas of nanoscience. This interest is spurred by the universal significance of chirality for chemistry, physics, biology, and medicine.[1,2] In this field, research on chiral nanoparticles (NPs) is further motivated by remarkably strong chiroptical effects,[3−5] unusual modes of chirality transfer,[6,7] the proximity of NP dimensions to biological chiral entities,[8] a multitude of possible catalytic processes taking place on their surfaces,[9,10] and self-organization phenomena.[6] The high polarizability and robustness of NPs make them a promising platform for polarization-based optical devices with significance for biosensing,[11,12] hyperspectral imaging,[13] and new information technologies.[14]

Noble metal[15−17] and II−VI semiconductor[18,19] NPs with chiral molecules on their surface are commonly used in many ongoing studies of chiral inorganic nanostructures.[1,20] Chiral forms of nanocarbon obtained by chiral separation[21−24] or direct

Received: February 10, 2017
Published: August 12, 2017

DOI: 10.1021/jacs.7b01445
J. Am. Chem. Soc. 2017, 139, 13701−13712

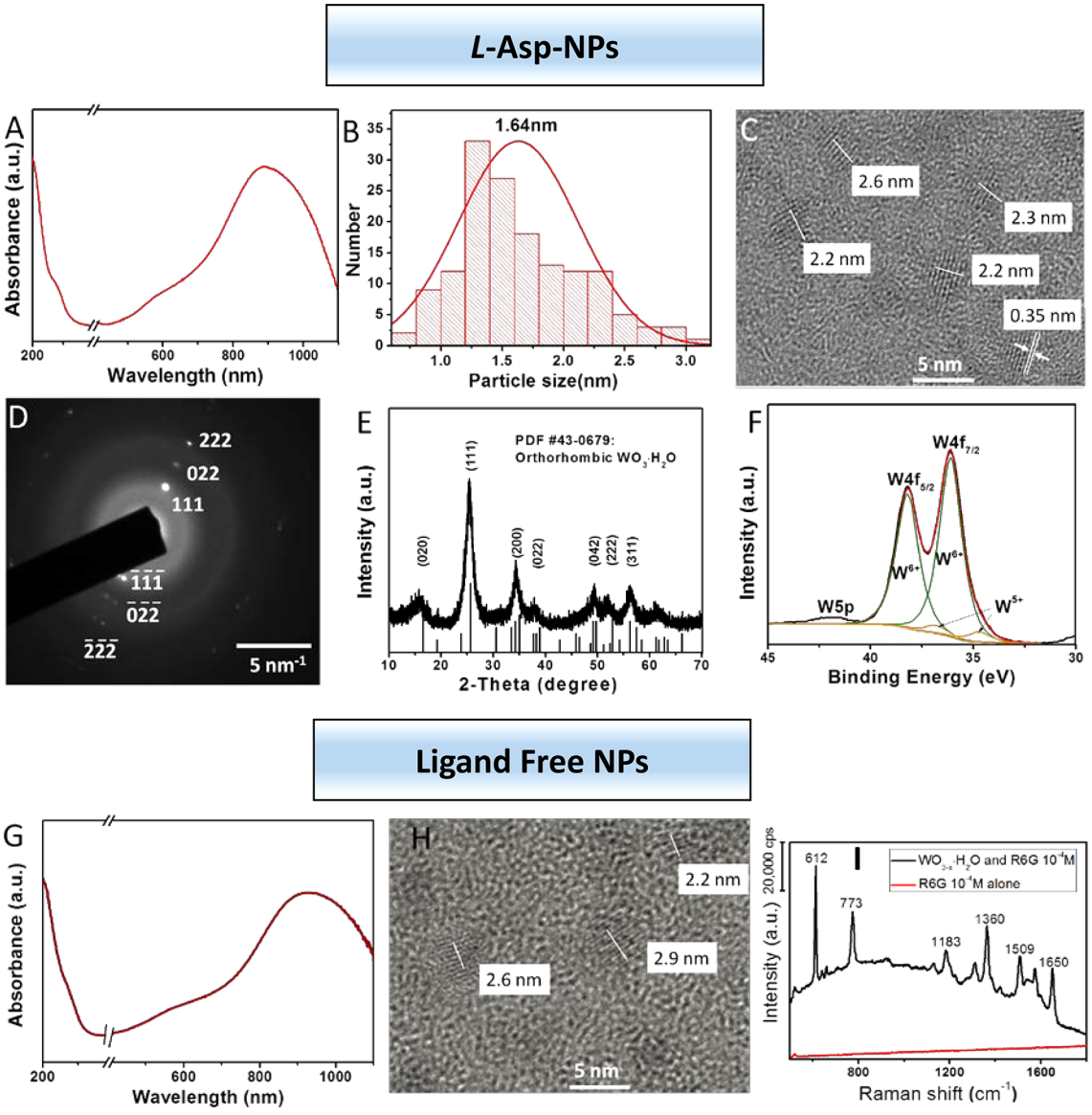

Figure 1. (A–F) Structure and properties of L-Asp-NPs of $WO_{3-x}\cdot H_2O$, $x = 0.03$. (A) UV–vis spectra of NP dispersions; spectra on the left and right of abscissa break are obtained for samples of 0.456 g L^{-1} ($[NP_{av}] = 3$ mmol L^{-1}) in a 1 mm-length cuvette and 0.304 g L^{-1} ($[NP_{av}] = 2$ mmol L^{-1}) in a 10 mm-length cuvette, respectively.(B) Size distributions derived from the TEM images of L-Asp-NPs. Total number of analyzed NPs is 150. (C) Representative high-resolution TEM image of L-Asp-NPs. (D) The corresponding electron diffraction pattern of NPs. (E) Powder XRD patterns of NPs. (F) XPS spectra with deconvoluted 4f peaks corresponding to two valence states of tungsten. (G, H) Structure and properties of ligand-free NPs of $WO_{3-x}\cdot H_2O$, $x = 0.03$. (G) UV–vis spectra of NP dispersions; spectra on the left and right of abscissa break are obtained for samples of 0.456 g L^{-1} (($[NP_{av}] = 3$ mmol L^{-1}) in a 1 mm-length cuvette and 0.304 g L^{-1} ($[NP_{av}] = 2$ mmol L^{-1}) in a 10 mm-length cuvette, respectively. (H) Representative high-resolution TEM image of ligand-free $WO_{3-x}\cdot H_2O$, $x = 0.03$ NPs. (I) Raman spectra of R6G (10^{-4} M) with and without ligand-free $WO_{3-x}\cdot H_2O$ NPs.

synthesis, for instance, carbon[25] and graphene[26] quantum dots, are also known. The chirality transfer from the chiral surface ligands to the inorganic core is typically used in the synthesis of different NP enantiomers.[27−29] Even when the ligands are not chiral, lattice defects exemplified by dislocations can serve as the source of asymmetry and distinct chiroptical activity in inorganic nanostructures.[30,31]

Ceramics represent some of the most common man-made[32,33] and natural nanomaterials.[34] Ceramic nanostructures are technologically essential for catalysis, medicine,[35] high-performance optics,[36] and some of the most fundamental questions in science, such as the origin of life.[37] These reasons motivated us to investigate methods of preparation and the properties of chiral ceramic NPs. Notably, only a few chiral ceramic materials have been prepared and investigated thus far.[38−41] Ceramic nanostructures with molecular chirality can be exemplified by silica fibers and nanotubes with helical channels or titania supraparticles with mesoscale porosity.[39,40] The chirality in these structures originates from the molecular imprinting of the organic templates on silica or titania during the sol–gel process. Although both oxides a wide band gap with electronic transitions in the UV range of the electromagnetic spectrum, silica gels exhibit chiroptical bands after incorporation of dyes and NPs active in the visible range.[40,42]

The adsorption of amino acids on different ceramic surfaces is well studied,[43−45] mainly due to the long-term interest in revealing the role of early earth minerals in the prebiotic formation of

DOI: 10.1021/jacs.7b01445
J. Am. Chem. Soc. 2017, 139, 13701−13712

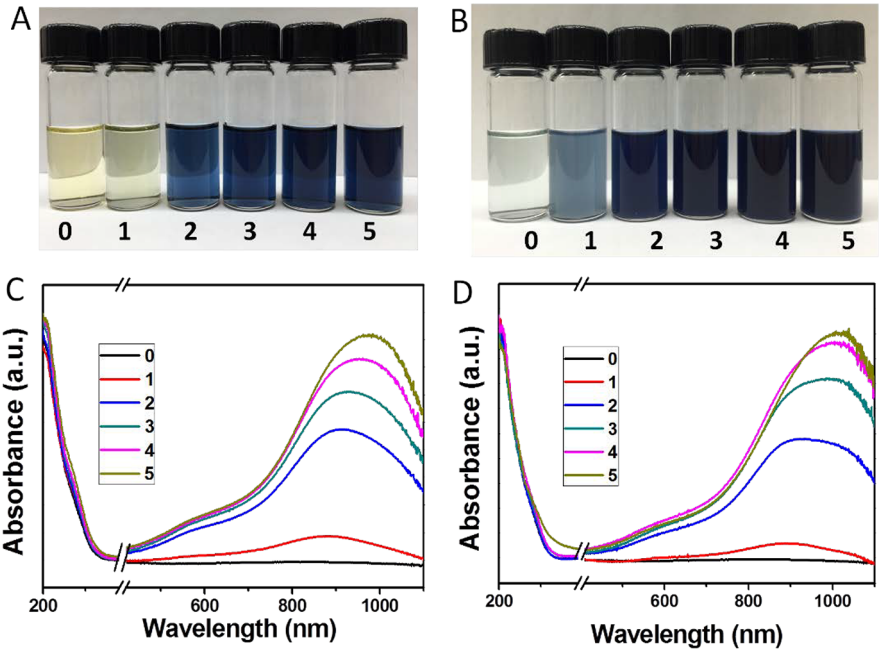

Figure 2. (A, B) Photographs of (A) 2.5 mL of L-Asp-NPs and (B) 2.5 mL of L-Pro-NPs in ethanol with different concentrations of water: 0, 0 mmol L^{-1}; 1, 22 mmol L^{-1}; 2 , 44 mmol L^{-1}; 3, 66 mmol L^{-1}; 4, 88 mmol L^{-1}; and 5, 110 mmol L^{-1}. (C, D) UV−vis spectra of NP dispersions; spectra on the left and right of abscissa break are obtained for samples of 0.456 g L^{-1} ($[NP_{av}]$ = 3 mmol L^{-1}) in a 1 mm-length cuvette and 0.304 g L^{-1} ($[NP_{av}]$ = 2 mmol L^{-1}) in a 10 mm-length cuvette, respectively. See Methods for calculation of size-averaged molar concentration of NPs denoted as [NPav].

peptides, proteins, and other biomolecules.[43,46−50] Early studies showed that adsorbed amino acids can be activated and go through condensation reactions (polymerization) after dry−wet or heating cycles.[48,51] Other studies demonstrated that amino acids bond to ceramic surfaces.[52−57] Although the role of inorganic surfaces in prebiotic peptide formation and stereospecificity of the bonds between amino acids and minerals are still in dispute,[58] it is likely that surface immobilization of amino acids facilitates the condensation reaction due to the inherent proximity of the reactants,[2] bond activation by coordination with mineral surfaces, and mitigation of the thermodynamic favorability of peptide bond hydrolysis.

Here we report the preparation and properties of ceramic NPs with an average diameter of 1.6 nm made from tungsten oxide hydrate, $WO_{3-x}{\cdot}H_2O$, which is known to have intense optical transitions from UV to near-infrared (NIR)[59,60] that can be associated with charge transfer,[61,62] plasmonic,[60,62,63] and polaronic[59,64−67] electronic transitions. The chirality of $WO_{3-x}{\cdot}H_2O$ NPs is imparted by the chirality transfer from surface ligands L- or D-aspartic acid (Asp) and L- or D-proline (Pro). In contrast with semiconductor,[68] metal,[69] and graphene NPs,[26] which would be expected to have nearly identical circular dichroism (CD) spectra for particles of the same size and shape, $WO_{3-x}{\cdot}H_2O$ NPs stabilized by Asp have remarkably different CD spectra compared with those stabilized by Pro. This spectroscopic effect is associated with the formation of double (Asp) rather than single (Pro) C−O−W bridges from dissociated carboxyl groups of the amino acid to the surface of the NPs. Correspondingly, chiral distortions of atomic packing on the surface of $WO_{3-x}{\cdot}H_2O$ alter the dominant electronic transitions responsible for the chiroptical maxima. The proximity of the surface ligands, activation of the amino groups, and favorable conditions for H_2O abstraction facilitate the condensation reaction between amino acid residue, that highlights the significance of the chiral $WO_{3-x}{\cdot}H_2O$ NPs for peptide synthesis and resolution its fundamental thermodynamic challenge.

RESULTS AND DISCUSSION

Synthesis and Characterization. Tungsten oxide NPs were prepared by arrested precipitation during solvolysis of WCl_6 dissolved in anhydrous ethanol in the presence of L- or D-Asp as well as L- or D-Pro. Addition of water, resulting in tungsten oxide hydrate, was found to be essential to obtain NPs with strong optical activity (see Supporting Information, Methods section). Thus, prepared NPs of tungsten oxide hydrate $WO_{3-x}{\cdot}H_2O$ stabilized by Asp and Pro will be denoted as Asp-NPs and Pro-NPs, respectively, with added L- or D-notation identifying the different enantiomer used in the synthesis. $WO_{3-x}{\cdot}H_2O$ NPs prepared from racemic (in the first approximation) mixtures of equimolar amounts of the corresponding enantiomers will be denoted here as *rac-* following the established conventions of organic chemistry. The limits of such a method of preparation of presumably racemic compounds and the possibility of chiral amplification from an undetectable excess of one enantiomer need to be noted.[70−72]

Thermogravimetric analysis (TGA) curves of $WO_{3-x}{\cdot}H_2O$ NPs display the weight loss inflections at ∼200 °C, ∼330 °C, and ∼530 °C (Figure S3). The first low-temperature weight loss is attributed to the release of the structural and physisorbed water in hydrated NPs. The second and third weight loss events are attributed to desorption and decomposition of Asp and Pro residues. For L-Asp, D-Asp, L-Pro, and D-Pro NPs, the amino acid content was calculated to be 16.8%, 18.1%, 11.6%, and 12.1%, respectively. In the molecular terms, these NPs carry approximately 15, 16, 11, and 12 moieties of corresponding amino acids per particle.

Conveniently, $WO_{3-x}{\cdot}H_2O$ NPs can be made in ethanol with and without amino acids. No significant difference in particle size, shape, composition, and UV−vis absorption spectrum was observed for the synthesis with and without amino acids (Figure 1A and 1G, 1C and 1H), which differentiates them from most metal and semiconductor NPs. This synthetic

DOI: 10.1021/jacs.7b01445
J. Am. Chem. Soc. 2017, 139, 13701−13712

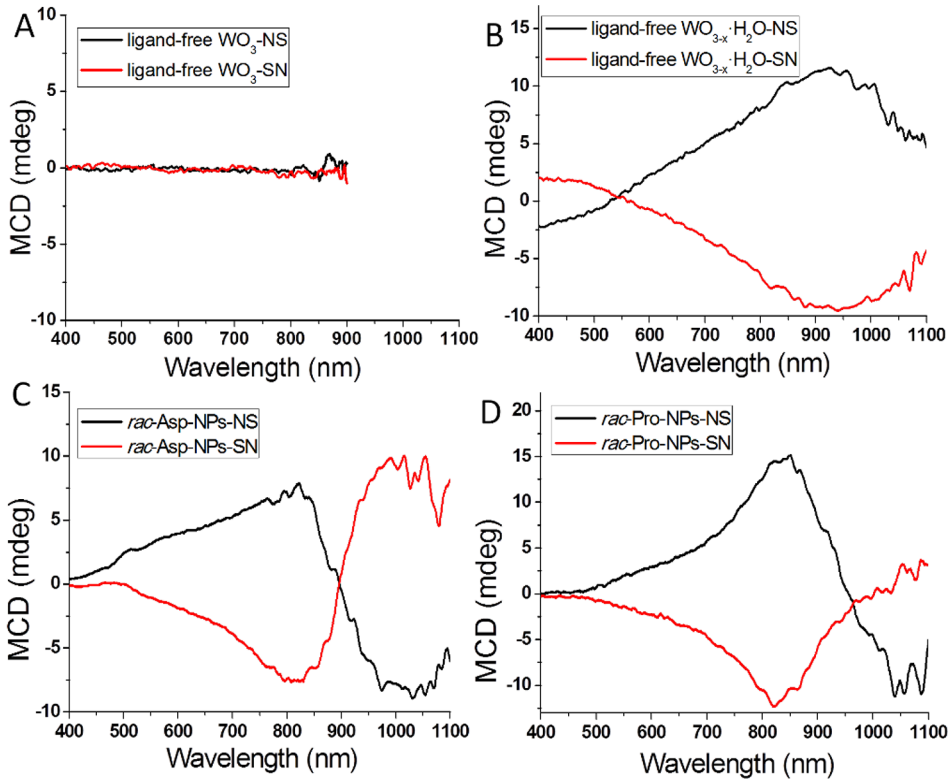

Figure 3. (A) MCD spectra of colorless, anhydrous, ligand-free WO_3 NPs. MCD spectra of (B) blue colored ligand-free $WO_{3-x}\cdot H_2O$ NPs, (C) *rac*-Asp-NPs, and (D) *rac*-Pro-NPs, respectively. Applied magnetic fields are +1.4 T (NS direction, black) and −1.4 T (SN direction, red). The concentrations of NPs were 0.95 g L^{-1} ($[NP_{av}]$ = 6.25 mmol/L, A-D) and the concentrations of added water were 33 mmol L^{-1} (B-D).

advantage of tungsten oxide NPs makes it feasible to discern various ligand effects experimentally. The NPs made without amino acid stabilizers will be referred to as *ligand-free* with the understanding that molecules of ethanol, water, and likely some ions are adsorbed onto the surface of tungsten oxide, providing kinetic stability to the NPs.

Transparent blue suspensions with nearly identical optical absorption spectra were obtained for all types of surface ligands. L-Asp-NPs of 1.9 g L^{-1} ($[NP_{av}]$ = 12.5 mmol L^{-1}) with water of 66 mmol L^{-1} (diluted as needed) are used as an illustrative example throughout the manuscript to discuss the properties.

The NP dispersions display an intense vis-NIR absorption band from 450 to 1100 nm with a maximum at 950 ± 50 nm and shoulder at ca. 580 nm (Figure 1A). Transmission electron microscopy (TEM) reveals that the NPs in these dispersions have an average size of 1.6 ± 0.5 nm (Figure 1B) and crystal lattice periodicity of 0.35 nm (Figure 1C). The lattice spacing, with periodicities of 0.35, 0.22, and 0.17 nm calculated from electron diffraction (ED) data (Figure 1D), is coincident with the (111), (022) and (222) crystal faces of $WO_{3-x}\cdot H_2O$. Furthermore, the X-ray diffraction (XRD) pattern of the L-Asp-NPs matches orthorhombic $WO_{3-x}\cdot H_2O$ (Figure 1E).[73]

X-ray photoelectron spectroscopy (XPS) provides essential information for understanding the elemental composition and optical properties of these ceramic NPs. The tungsten 4f region of XPS spectra (Figure 1F) reveal that NPs contain both W^{6+} and W^{5+} oxidation states. XPS peaks at 36.1 and 38.2 eV correspond to W^{6+}, while the peaks at 34.7 and 36.8 eV correspond to W^{5+}. The spin−orbital doublet splitting of 2.1 eV and an area ratio of 4:3 are characteristic for both ions.[74−77] Thus, the cumulative chemical formula for the NPs is $WO_{3-x}\cdot H_2O$ with x = 0.03 calculated from the ratio of the XPS peaks.

Optical Absorption and Electronic Transitions. The light absorption of $WO_{3-x}\cdot H_2O$ NPs is found in the region from 450 to 1100 nm. This strong, broad light absorption band is observed for both ligand-free and amino acid-coated NPs (Figure 1A and 1G) when a controlled amount of water is added to ethanol. The dispersions prepared in anhydrous ethanol are colorless (Figure 2A and 2B). A finely controlled increase of water content deepens the blue color and increases the intensity of the near IR band with a maximum at 950 ± 50 nm for both L-Asp-NPs and L-Pro-NPs. Addition of excess of water results in bleaching and concomitant precipitation of NP agglomerates. The absorption peaks in the UV region attributed to amino acids (Figure S4) do not change with increasing amounts of water (on left of the abscissa break in Figure 2C and 2D); the broadening of these peaks compared with those from free amino acids is associated with the variability of dielectric environment on the surface of the NPs.[78]

To better understand the nature of the electronic processes in ligand-free and amino-acid-modified $WO_{3-x}\cdot H_2O$ NPs, we employed magnetic circular dichroism (MCD) spectroscopy as technique complementary to UV−vis spectroscopy to isolate individual components of complex light absorption bands. MCD records CD spectra of the sample placed in magnetic field that results in Zeeman splitting of excited/ground states and accompanying mixing of states induced by magnetic field. This experimental technique is often used to study nonreciprocal electromagnetic effects in chiral and nonchiral media. Here, MCD spectroscopy was carried out on *rac* samples of *rac*-Asp-NPs and *rac*-Pro-NPs that did not show standard CD peaks (Figure S5). The near-racemic dispersions were chosen on purpose in order to avoid overlap of two types of chiroptical activities complicating the interpretation of the spectra. Under these conditions, MCD spectra

DOI: 10.1021/jacs.7b01445
J. Am. Chem. Soc. 2017, 139, 13701−13712

enable the researcher to identify the electronic transitions better than traditional UV−vis spectroscopy due to the sharpness of the MCD peaks discriminating between different types of electronic transitions based on the variable contributions of the non-reciprocal effects.

MCD spectra were taken in the Faraday geometry for S-to-N and N-to-S directions of the magnetic field aligned with the propagation vector of the light beam. Similar to the UV−vis spectra in Figure 2C, curve 0, corresponding to the colorless ligand-free WO_3 sample made in anhydrous ethanol (Figure 3A), shows no MCD peaks in the visible range. These baseline spectra indicate that there is no artifactual birefringence associated with particle alignment on the walls or in solution that may occur spontaneously.[79] The ligand-free $WO_{3-x}{\cdot}H_2O$ NPs display strong MCD peaks in NIR range with a maximum at ca. 940 nm and a shoulder at ca. 750 nm (Figure 3B), indicating that multiple transitions contribute to MCD phenomena in these NPs. The nonderivative shape of the peak in NIR part of the spectrum is indicative of the magnetic-field-induced hybridization of closely spaced electronic states that are not resolved in the UV−vis spectrum (Figure 1G), although a more detailed study including the possibility of the Zeeman splitting of the ground state is waranted.[80]

The MCD spectra of *rac*-Asp-NPs differ substantially from those of ligand-free NPs. The distinct bisignate MCD peaks appearing at ca. 830 and 1040 nm in *rac*-Asp-NP are prominently featured in the MCD spectra (Figure 3C). The derivative shape of the spectrum in the NIR part with intersection at ∼900 nm indicates that Zeeman splitting of the excited state, corresponding to the 900 nm peak in Figure 1C, is responsible for the MCD spectrum in NIR in NP bearing surface ligands. Adsorption of the amino acids drastically changed the energy of the surface states that can no longer effectively hybridize with the main NIR transition, which points to the pivotal role of the surface states on the lattice of WO_{3-x} for optical properties of Asp-NPs. Compared with other NPs,[81,82] the involvement of multiple electronic states with markedly different transient magnetic moments can also be inferred.

Confirming these points, *rac*-Pro-NP dispersions display strikingly different MCD peak patterns compared with *rac*-Asp-NPs despite the nearly identical shape of UV−vis spectra in Figure 2C and 2D. The peak in the NIR range at 1040 nm is weaker than that at 830 nm for *rac-Pro*-NPs (Figure 3C and 3D). The new surface states altering the MCD spectrum are likely to be associated with the pyrrolidine ring in Pro. Based on the markedly increased intensity of the MCD peak at 800 nm, one can envision the increased hybridization of electronic states WO_{3-x} and those of pyrrolidine ring of Pro compared with the aliphatic skeleton of Asp.

The stark spectral differences between amino-acid-modified and ligand-free $WO_{3-x}{\cdot}H_2O$ NPs as well as the marked changes of intensity in MCD bands for Asp-NPs and Pro-NPs suggest that the amino acid layer plays a significant role in the genesis of these bands. Most changes of MCD signatures between Asp-NP and Pro-NP occur in the visible part of the spectrum, that is, wavelength shorter than 800 nm, which allows us associate this spectral diapason with electronic transitions associated with the amino acid layer. The presence of the cross-sectional point at ∼900 nm and the derivative shape of the MCD band in NIR part for both Asp-NP and Pro-NP juxtaposed on the strong MCD peak at ∼900 nm for ligand-free NPs point to the fact that the electronic transitions in the 900−1100 nm window are associated with ceramic core of the NPs with some influence from the adsorbed amino acids.

To understand better the implications of the structural asymmetry on the optical activity of $WO_{3-x}{\cdot}H_2O$ NPs, it is useful to discuss the origin of absorption bands in tungsten oxide nanomaterials. Metal-to-ligand charge transfer (MLCT) bands are well-known for many ceramic surfaces[83,84] and can be firmly associated with the 500−700 nm absorption bands of $WO_{3-x}{\cdot}H_2O$ NPs in the visible range (Figure 1,2). The possible origin of the bands in the red and NIR parts of the spectrum is more complex.[63] The electronic state responsible for 800 nm is ligand-dependent (Figure 3B−D) and may be attributed to MLCT transition, but the electronic state responsible for 1000 nm is weakly affected by the surface ligand (Figures 1−3) and dependent mostly on the chemistry of the ceramic core and its hydration state, in particular. Two types of electronic transitions can be associated with excited states with energies around 1 eV for tungsten oxide: the plasmons[60,62,63] and polarons.[59,64−67] Plasmons represent oscillations of electronic charge density in the volume of the entire NP. Polarons represent local charge transfer between the W^{5+} and W^{6+} sites.[65,66] Let us consider the possibility of both of these transitions in $WO_{3-x}{\cdot}H_2O$ NPs.

Addition of water to the colorless anhydrous WO_3 sample (Figure 2A, B, curves 0) results in the formation of oxygen vacancies[85−87] (see Supporting Information) that represent local excesses of electrons and accumulate at the $WO_{3-x}{\cdot}H_2O$ surface. In another perspective, it can be treated as the reduction of a portion of W^{6+} ions to W^{5+} ions resulting in the possibility of $W^{5+} \rightarrow W^{6+}$ electron transfer upon photoexcitation.[88,89] Simultaneously, the electrons from oxygen vacancies can be injected into the solid-state electronic bands associated with the tungsten oxide lattice that encompass the entire NP. This delocalization makes these electrons more mobile and can result in their coherent oscillations, constituting plasmons.

Attribution of the NIR band in tungsten oxides to polarons is broadly accepted.[64,65] Since the possibility of plasmons is less known for ceramic materials,[60] we tested whether or not some of the electronic transitions observed in UV−vis spectra and MCD were consistent with plasmonic excited states. The observation of surface-enhanced Raman scattering (SERS) is associated with plasmonic nanostructures capable of generating so-called "hot-spots". The latter represent locally enhanced electrical fields and have been extensively reported for the archetypal plasmonic nanostructures from noble metals, graphene, and even Cu_2S.[26,90−92] The SERS spectrum of Rhodamine 6G (R6G) is obtained under excitation with a 532.8 nm wavelength laser when the dye was mixed with ligand-free $WO_{3-x}{\cdot}H_2O$ NPs (Figures 1I and S6). The SERS peaks of R6G were observed at 612, 773, 1183, 1360, 1509, and 1650 cm^{-1} and match previously reported values.[93] This observation is consistent with the plasmonic nature of the absorption bands in our NPs.[93,94]

Considering the optical absorption spectrum as a plasmon resonance spectrum, we performed simulations with the Mie−Gans theory. The calculated vis-NIR absorption spectrum of our WO_{3-x} NPs shows a reasonably good match with the experimental spectrum (Figure S2), indicating the plausibility of plasmon excitation states in $WO_{3-x}{\cdot}H_2O$ NPs. Furthermore, the absorption spectra in solvents with various refractive indices[95] display batochromic shifts of the plasmon peak with increasing refractive index, which is typical for plasmons.

Plasmons and polarons are not mutually exclusive. The overlap of two or more electronic processes producing red and NIR bands was also recognized in MCD spectra (Figure 3).

DOI: 10.1021/jacs.7b01445
J. Am. Chem. Soc. 2017, 139, 13701−13712

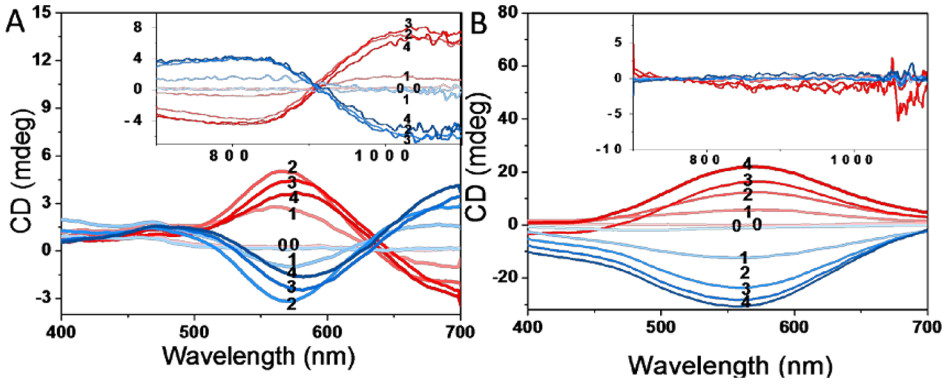

Figure 4. CD spectra of (A) L- and D-Asp-NPs (red and blue, respectively) (inset: NIR range of corresponding CD spectra) and (B) L- and D-Pro-NPs (red and blue, respectively) (inset: NIR range of corresponding CD spectra) containing different concentrations of water: 0, 0 mmol L^{-1}; 1, 22 mmol L^{-1}; 2, 44 mmol L^{-1}; 3, 66 mmol L^{-1}; and 4, 88 mmol L^{-1}, respectively.

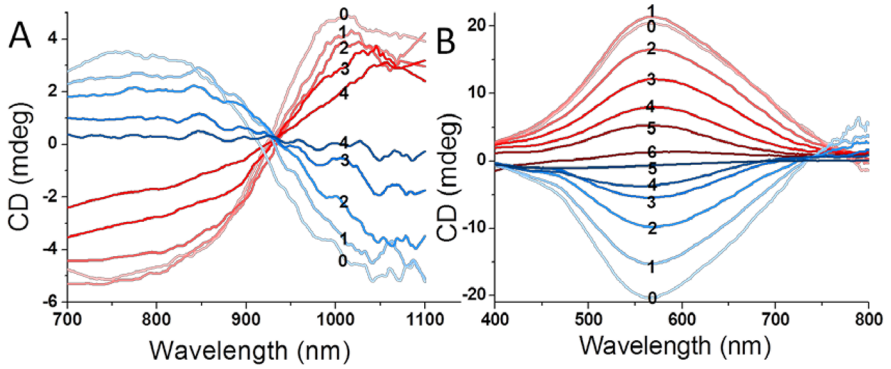

Figure 5. CD spectra of (A) L- and D-Asp-NPs (red and blue, respectively) after addition of H_2O_2 in different concentrations: 0, 0 mmol L^{-1}; 1, 0.03 mmol L^{-1}; 2, 0.06 mmol L^{-1}; 3, 0.09 mmol L^{-1}; and 4, 0.12 mmol L^{-1}, respectively. (B) L- and D-Pro-NPs (red and blue, respectively) after addition of H_2O_2 in concentrations of 0, 0 mmol L^{-1}; 1, 0.06 mmol L^{-1}; 2, 0.12 mmol L^{-1}; 3, 0.18 mmol L^{-1}; 4, 0.24 mmol L^{-1}; 5, 0.30 mmol L^{-1}; and 6, 0.36 mmol L^{-1}, respectively.

Therefore, we consider that both of these states have oscillation strength in the 800−1100 nm spectral range, while MLCT electronic transitions are active in 500−700 nm range in WO_{3-x}·H_2O NPs.

Chiroptical Activity. Similarly to free L- and D-Asp with symmetrical CD peaks at 200 nm (Figure S7A), both L- and D-Asp-NPs reveal classical mirror-image CD spectra (Figure 4A). After conjugating with WO_{3-x}·H_2O NPs, the original CD peaks of L- and D-Asp shift to 210 nm and become broader due to the interaction with the ceramic surface (Figure S7C).

In the anhydrous NPs, no CD signals appear with either type of amino acid in the 400−1100 spectral range. The intensity of the chiroptical bands gradually increases over the entire vis-NIR range as a specified amount of water is added to the dispersion (Figure 4). An excessive amount of water causes aggregation and discoloration. The disappearance of the NIR band in CD spectra is attributed to neutralization of oxygen vacancies. Asp-NPs containing 66 mmol L^{-1} of water (Figure 4A) and Pro-NPs containing 88 mmol L^{-1} of water displayed the most intense polarization rotation (Figure 4B).

L- and D-Asp-NPs showed chiroptical activity over the entire spectral range of 200−1100 nm (Figure 4A) with a *g*-factor describing chiroptical asymmetry not higher than 3.5×10^{-4} (Figure S8B). The characteristic chiroptical bands of L- and D-Pro associated with the $\pi \rightarrow \pi^*$ transitions, with peaks at 197 and 217 nm (Figure S7B), underwent a red shift to 202 and 228 nm, respectively, after being attached to WO_{3-x}·H_2O NPs. In addition, two new CD peaks emerged at 274 and 301 nm for Pro-NPs (Figure S7D). Based on the previous theoretical and experimental studies of Pro, poly(Pro), and Pro segments in proteins,[96−100] one can state that the appearance of these two bands is not associated with conformation of the molecule but rather with the influence of ceramic surface on the $\pi \rightarrow \pi^*$transitions in the pyrrolidine ring of Pro. A strong coordination of the nitrogen atom with WO_{3-x} surface is anticipated, which correlates well with conclusions made from the MCD data in Figure 3D. Multiplicity of the surface states with the different degree of bonding to the NP core that could be responsible for the two new chiroptical peaks in Pro and broadening of the $\pi \rightarrow \pi^*$ chiroptical peak in Asp must be pointed out.

In the visible part of the spectrum, L- and D-Pro-NPs showed a pronounced, broad chiroptical band at 560 nm, similar to Asp-NPs' peaks in terms of shape, range, and maximum peak, with the highest intensity of −30 mdeg and the highest *g*-factor of 1.83×10^{-3} in the visible region (Figures 4B and S8D). The corresponding *g*-factor curves of UV range are shown in Figure S8A, C. The chiroptical activity in the NIR range is weak compared to that in UV−vis range for the same NPs, although it is comparable to CD intensity in NIR for L- and D-Asp-NPs.

From the previous section, one can infer that the presence of oxygen vacancies (and thus the excess of electrons) in the NPs results in strong optical absorption.[85−87] Therefore, addition of oxidants should reduce the optical activity.[101,102] Indeed, the addition of H_2O_2 decreased the absorption intensity and chiroptical activity of L- and D-Asp-NPs (Figures 5A and S9A). The same was observed with L- and D-Pro-NPs (Figures 5B and S9B).

DOI: 10.1021/jacs.7b01445
J. Am. Chem. Soc. 2017, 139, 13701−13712

Other reagents capable of withdrawing electrons from tungsten oxide act in the same way, including Au^{3+}, MnO_4^-, and ClO_4^-. Furthermore, the much milder oxidizers Fe^{3+}, Cu^{2+}, $S_2O_8^{2-}$, and SO_3^{2-} act in the same way, which lends these NPs to future studies of chiral redox catalysis. The addition of an oxidant to the same volume of ligand-free $WO_{3-x}\cdot H_2O$, L- and D-Pro-NPs, and L- and D-Asp-NPs led to the rapid loss of color (Figure S10). As expected, the CD and absorption intensity of Pro-NPs and Asp-NPs disappear as well (Figure S11).

In order to better understand the differences in chiroptical properties of the two types of coated NPs, we looked into the chemical bonding mode of Asp and Pro with $WO_{3-x}\cdot H_2O$. Fourier-transformed infrared (FTIR) spectroscopy unearthed a large amount of data rich in structural information about the nature of the NP surfaces. The C═O and C−O stretching vibration bands appear at 1725 and 1207 cm^{-1} in the case of Asp-NPs and at 1735 and 1220 cm^{-1} for Pro-NPs (Figures 6 and S1).

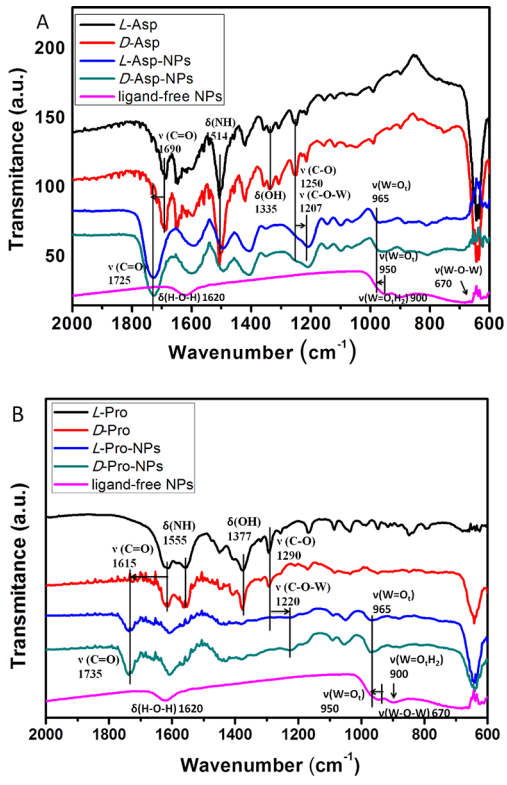

Figure 6. FTIR spectra (2000−600 cm^{-1}) of (A) L- and D-Asp, L- and D-Asp-NPs, and ligand-free $WO_{3-x}\cdot H_2O$ NPs and (B) L- and D-Pro, L- and D-Pro-NPs, and ligand-free $WO_{3-x}\cdot H_2O$ NPs.

The frequency of ν(C═O) increased, whereas that of ν(C−O) decreased after being bound to NPs, which is consistent with the formation of coordination bonds between an oxygen atom of the carboxyl group in the amino acid and the tungsten on the NP surface.[103] The tungsten−oxygen bond causes electron density to shift away from the O atom, weakening the C−O bond and lowering the frequency of the ν(C−O) stretching vibrations. Concomitantly, the C═O bond becomes stronger due to an additional electrostatic component and ν(C═O) moves to higher frequencies. A similar change can be observed for the stretching band of W−O_t at 950 cm^{-1}, which undergoes a shift to 965 cm^{-1} with the formation of W−O bonds in the C−O−W bridges between the Asp/Pro and NP surface.

The bands at 1335 cm^{-1} for Asp and 1377 cm^{-1} for Pro correspond to the bending vibrations of the carboxyl O−H group.[104,105] These bands nearly disappeared during the course of the NP synthesis (Figure 6), which confirms the formation of the C−O−W linkage between the amino acids and $WO_{3-x}\cdot H_2O$. While several coordination modes can be considered for carboxyl groups with tungsten ions,[103,106] our cumulative assessment of FTIR and optical spectroscopy data in Figures 3−5 leads to the conclusion that a carboxyl C−O unit coordinates with a tungsten ion on the NP surface as a monodentate ligand. Both −COOH groups of Asp are presumed to have dissociated and coordinated with the NPs, since no evidence of nondissociated carboxyl groups can be found for Asp (Figure 6). The second carboxyl group of Asp is likely to be under strain and bind more weakly with a tungsten ion, which, besides other factors, manifests in greater broadening and smaller shifts of the FTIR bands for Asp than for Pro, for instance, for the ν(C═O) or ν(C−O) stretching vibrations. The presence of two C−O−W linkages between the Asp moiety and $WO_{3-x}\cdot H_2O$ also correlates with the differences observed in the MCD spectra in Figure 3, displaying double and single peaks for Asp-NPs and Pro-NPs, respectively. These peaks are indicative of both the energy and symmetry of the electronic states associated with the ligand shells of the two types of NPs.

Coordination of the surface tungsten atoms with the lone pair of the amino acid nitrogen atom is also possible and can be visualized by the appearance of new CD peaks at 274 and 301 nm (Figure S7) for Pro-NPs. FTIR spectra indicate that the δ(N−H) band at 1514 cm^{-1} for the $-NH_2$ group of Asp is broadened and shifted to lower frequencies, indicating interactions with the NP surface. The same can be said for the −NH group of Pro, whose weak δ(N−H) band at 1555 cm^{-1} nearly disappears when NPs are formed. Since the average energy of these vibrations remains mostly the same, nitrogen atoms have a weaker and perhaps more dynamic coordination with the NP surface than the oxygen atoms of carboxyl groups. Hydrogen bonding with neighboring amino acid molecules, for instance, the oxygen atoms of the C═O groups, needs to be considered as well.

Current knowledge about the chemical bonding between the amino acid residues and the ceramic core provides arguments to account for the differences in chiroptical spectra between Asp- and Pro-NPs. The prevailing understanding of chirality in individual NPs is based on the chirality transfer from the organic shell to the inorganic core via deformations of the atomic packing of the crystal lattice by the chiral organic shell.[2,19,68,69,107−110] In fact, this mechanism has a lot of similarities with other cases of nanoscale chirality observed in supramolecular chemistry.[111] Additional chemical mechanisms leading to chirality of NPs are also possible.[20,29] For instance, the observed chiroptical activity can be associated with polarization effects[17] that are likely in plasmonic NPs.[20,112] Similarly to proteins, the shape of the NPs as a whole can also be chiral[18] and necessarily results in a difference in absorption of left- and right-circularly polarized light.[5] Higher-order chiral geometries may also emerge for NP assemblies[3,20,28,113] and are likely to lead to even stronger optical activity.

In our case, TEM images (Figure 1) indicate that NPs are small with nearly spherical geometry. The entire NPs can be asymmetric and potentially chiral when distinct three-dimensional deviations from nearly perfect centrosymmetric geometry are present.[20] However, we examined over 150 TEM images of individual NPs and found that they generally appear as largely centrosymmetric shapes. Therefore, the geometry of the

DOI: 10.1021/jacs.7b01445
J. Am. Chem. Soc. 2017, 139, 13701−13712

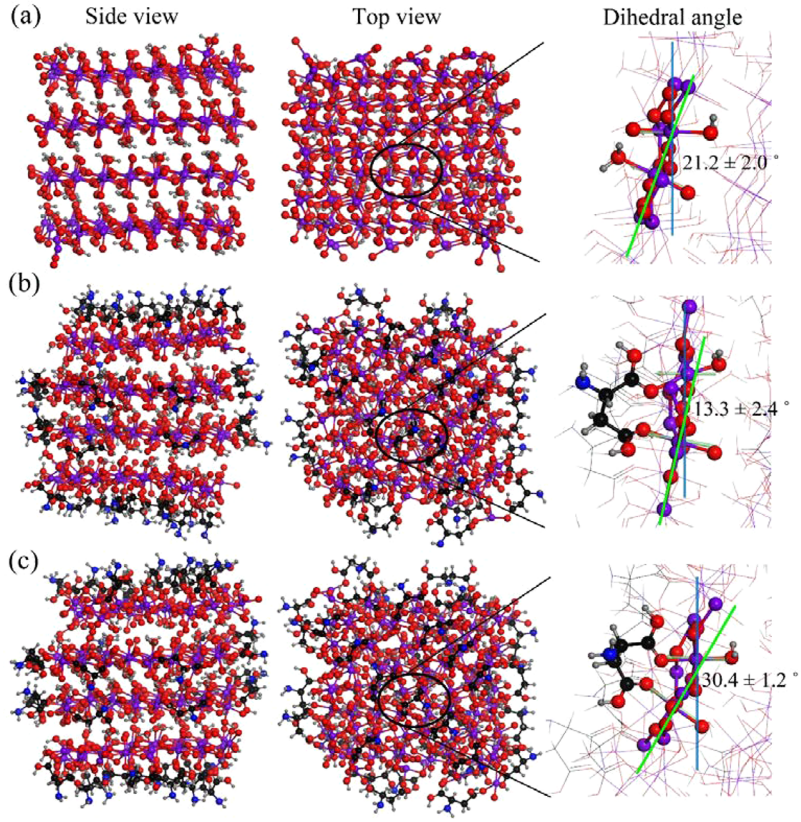

Figure 7. MD simulations of the atomic structure in the minimum energy state for (A) ligand-free, (B) L-Asp, and (C) D-Asp NPs.

inorganic cores of the NPs as a whole is likely to contribute less than other factors to the chiroptical activity observed in dispersions (Figures 4 and 5). Since the addition of water to premade NPs transforms them from being chiroptically silent to being chiroptically active (Figure 4) and the reversal of this effect by addition of H_2O_2 (Figure 5) results in no discernible variation in TEM shapes (Figure S12), chiral geometries responsible for chiroptical activity in Figure 4 are found in these NPs at the molecular scale. Therefore, surface distortions caused by the layers of Asp and Pro emerge as the most probable source of chirality in these NPs and the primary structural factor responsible for the CD peaks. The distortions of the inorganic phase inevitably affect the oxygen vacancies imbedded in WO_{3-x} lattice and all the electronic transitions associated with them.

The difference in the binding of the amino acids to NPs has direct consequences for the shape, range, and relative intensity of CD bands (Figure 4), which helps one to rationalize the differences in chiroptical properties of the Asp- and Pro-NPs. The double-point binding of Asp to $WO_{3-x}{\cdot}H_2O$ core through its two carboxyl groups causes stronger distortion than single-point binding via the single carboxyl group of Pro. Considering that the chiroptical activity of Asp-NP peaks in the NIR part of the spectrum, this observation matches well with the attribution of the 1050 nm band to a polaron/plasmon transition. The binding of Pro via a single −COOH group and distant coordination of −NH group in the pyrrolidine ring apparently affects the same electronic transitions characteristic of the NP core to a smaller extent. Therefore, the Pro-NPs display weak chiroptical bands in NIR, but have a strong peak at higher energies at 560 nm that can be associated with surface states and MLCT transitions involving surface-bound molecules other than amino acids, as the same UV−vis band can also be observed in ligand-free NPs (Figure 1G).

Molecular Dynamic Modeling. The attribution of the chiroptical effects for Asp-NPs at 1050 nm in NIR part of the spectrum to chiral distortions of the $WO_{3-x}{\cdot}H_2O$ is significant for further development of chiral inorganic nanomaterials with expanded palette of chemical and physical properties. Therefore, we decided to confirm the conclusion about the chirality transfer from amino acids to ceramic WO_{3-x} lattice made on the basis of chiroptical properties by molecular dynamics (MD) simulations. MD toolbox in conjunction with electron microscopy and spectroscopic data offers numerous research venues for NP studies. The choice of the MD methods and force fields is strongly dependent on the questions posed for these simulations. In this study, we sought the answers to the following question that would prove or disprove the presence of atomic scale chirality of the ceramic core of the NPs: Can amino acid residues attached to the NP surface produce chiral distortions of the crystal lattice of $WO_{3-x}{\cdot}H_2O$?

The ligand-free model of the $WO_{3-x}{\cdot}H_2O$ NPs with the lateral size of 1.9 × 2.0 × 2.2 nm with a quasi-cubic shape (Figure 7) was constructed using Forcite Plus module in Materials Studio. Universal force field (UFF) that includes potentials for tungsten atoms was used to describe the atomic motion of the constituent atoms. L- and D-Asp residues were attached to the surface of WO_{3-x} in accord with the double-point binding identified from FTIR and other data (Figures 6 and S12). The atomic geometry of the NPs was allowed to relax to the equilibrium states L- and D-Asp for 20 and 100 ns. The energy of the structure remains constant within the simulation error after 20 ns (Figure S12). These data indicate that the crystal lattice distortions are thermodynamic in nature.

The obtained MD models of L- and D-Asp NPs show that the packing of tungsten oxide lattice is distorted after L/D-Asp is

DOI: 10.1021/jacs.7b01445
J. Am. Chem. Soc. 2017, 139, 13701−13712

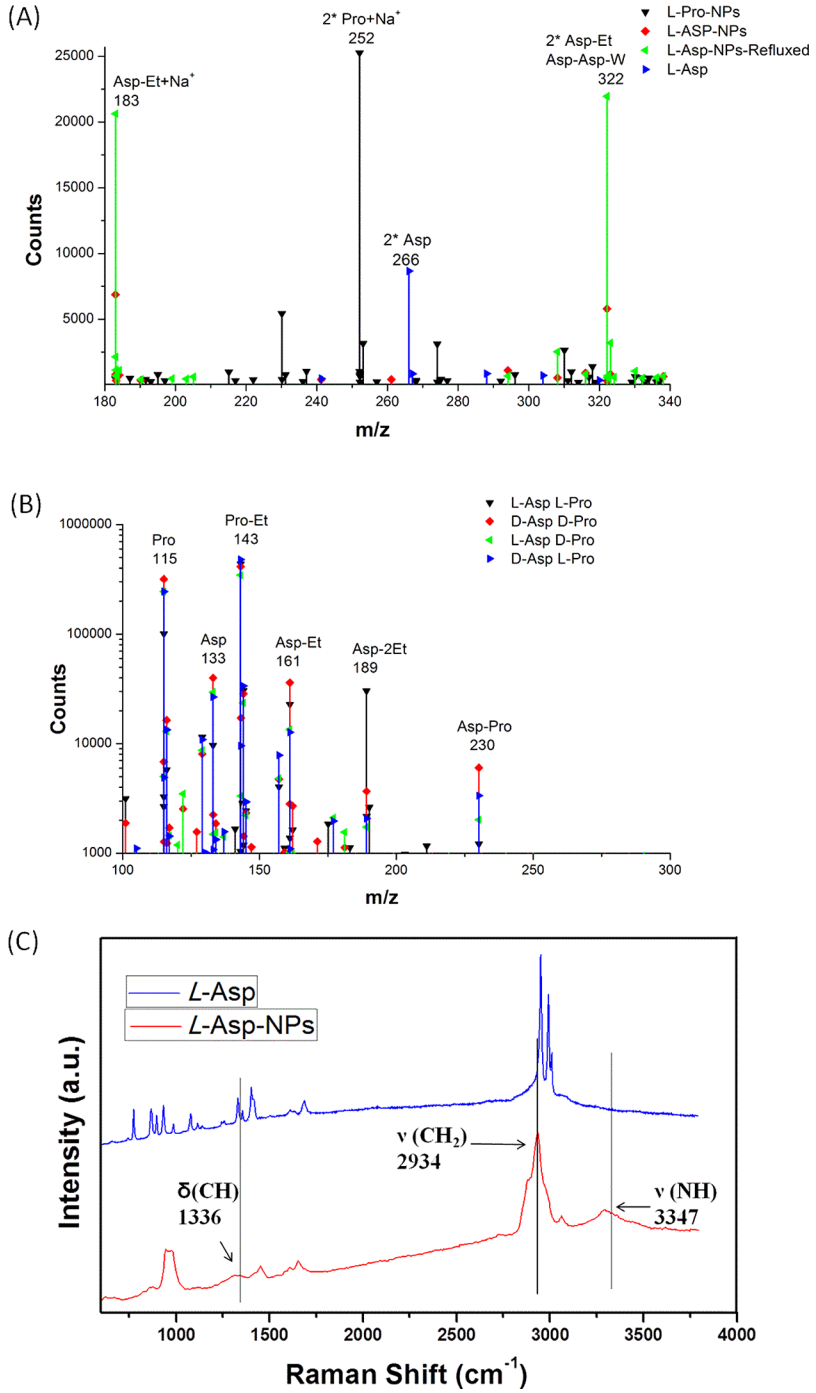

Figure 8. Monoisotopic mass spectra obtained for L-Pro-NPs /L-Asp-NPs, L-Asp NPs, and L- Pro NPs dried at 70 °C. Samples denoted as L-Asp-NPs-Refluxed were prepared by refluxing at 78 °C for 5h prior to precipitation and drying at room temperature. (B) Monoisotopic mass spectra of amino acids and peptides formed on NPs carrying both Pro and Asp after precipitation and drying at 70 °C for 12 h. All MS spectra were obtained for trifluoroacetic acid (TFA) extracts from the NP samples (see Supporting Information, Methods section). Notations: Asp-Asp denotes the dipeptide formed by two Asp molecules, Asp-Pro denotes the aspartic acid and one proline molecule, Asp-Et and Pro-Et denote aspartic and proline ethanol ester, respectively, and Na+ and W denote sodium ion and tungsten atom adducts to other residues, respectively, forming in the gas phase of MS spectrometers. (C) Raman spectroscopy of pure L-Asp and L-Asp-NPs prepared by refluxing at 78 °C for 5 h.

adsorbed in the WO_3 surface Asp (Figure 7) compared to the ligand-free NPs. The distortions are sufficient to affect the chiroptical activity associated with both plasmonic and polaronic states. MLCT states will certainly be affected because they involve the amino acid ligands. We must note, however, that calculations of the chiroptical spectra from atomistic models in Figure 7 would be highly desirable. However, the limitations of the quantum mechanical methods for NPs made from large number of atoms make it difficult to realize using both ab initio and density functional theory toolboxes. Their rapid development is likely to make this research task possible in the near future.

Catalytic Activity. The mineral surface of ceramic nanostructures, that is, $WO_{3-x}{\cdot}H_2O$ NPs, can be catalytic. Under-

DOI: 10.1021/jacs.7b01445
J. Am. Chem. Soc. 2017, 139, 13701−13712

coordinated metal and oxygen atoms increase the retention time of the reagents at the surface and change the interaction energy barriers.[114] Herein, we explored the catalysis of peptide-bond formation involving amino acids on $WO_{3-x}\cdot H_2O$ NPs. Our interest in this reaction and the possibility of its facilitation by chiral ceramic NPs is motivated by both fundamental and practical reasons. The former are represented by the wide range of long-standing questions related to the origin of life.[37,49,50,115−117] Our practical interest in the catalytic activity of chiral ceramic NPs relates to their importance in the synthesis of peptides for medicine and other purposes.[118] $WO_{3-x}\cdot H_2O$ NP dispersions are attractive from the perspective of scalable peptide synthesis because of the low cost and robustness of ceramic NPs, which can potentially replace homogeneous enzymatic catalysts. The simplicity of separation and reuse is also a distinct advantage of NP-based heterogeneous catalysts. Last but not the least, the alcoholic media used to synthesize WO_{3-x} NPs can facilitate condensation reactions by reducing the chemical potential of abstracted water, thereby shifting the thermodynamic equilibrium toward peptides.[119] The unfavorable thermodynamics of peptide-bond formation is one of the central chemical problems for this type of reaction.[43]

Thus, we tested whether $WO_{3-x}\cdot H_2O$ NPs carrying Asp and/or Pro on the surface can facilitate the formation of dipeptides in the framework of thermal catalysis. We either refluxed the dispersion of NPs at 78 °C for 5h prior to drying at room temperature or heated to drying at 70 °C for 12 h after precipitation. Mass spectroscopy and Raman spectroscopy were used to identify the products according to the protocol given in the Supporting Information, Methods section.

The catalytic formation of dipeptides was investigated for L-Asp-NPs and L-Pro-NPs as well as NPs carrying the equimolar mixture of different amino acids, with the corresponding CD spectra shown in Figure S14. Considering the spectrum of conditions that were used in the past, with reaction times of up to several tens of days[117] and heating with temperatures as high as 100, 130, and even 190 °C,[120−122] the conditions used herein are mild, and the duration of the reaction is short.

The formation of an Asp-Asp ethanol ester with a mass of 276 au is observed for L-Asp-NPs (Figure 8A). Although no Pro-Pro dipeptides are found for L-Pro-NP, a relatively high amount of an Asp-Pro dipeptide with a mass of 230 au is found for NPs that carry both Asp and Pro (Figure 8B). The lack of Pro-Pro dipeptides is likely to be associated with the coordination of nitrogen in the pyrrolidine with the surface of WO_{3-x} discussed above (Figures 3D, 4, 6B, and S7). Different permutations of the chirality of the amino acids were tested for NPs with mixed surface ligands. Although some differences were observed, it would be premature at the moment to discuss them.

The degree of esterification in the presence of NPs was also enhanced in comparison with samples without any NPs (Figure 8A). From these data we conclude that binding to WO_{3-x} surface facilitates formation of dipeptide bonds involving Asp either with the same or different amino acid. The degree of specificity in respect to Asp is associated with the double coordination with the WO_{3-x} surface because electrophilic activation of the carbon atoms in carboxyl groups by bonding with ceramic surface (Figure 7) facilitates the formation of C−N bond with unpaired electrons of nitrogen in the amino groups.

The formation of peptide bonds is confirmed by Raman spectroscopy (Figure 8C). The new peaks at 2934, 3347, and 1336 cm^{-1} appear, corresponding to the dipeptide of Asp.[123] The peaks at 3347 and 2934 cm^{-1} indicate the stretching vibrations of NH and CH_2, while the peak at 1336 cm^{-1} is attributable to bending vibrations of the CH group.

CONCLUSIONS

Chiral ceramic NPs have been prepared by arrested precipitation of tungsten oxide in alcohol in the presence of two natural amino acids: Asp and Pro. UV−vis, CD, MCD, and FTIR spectroscopy indicate that these NPs feature two chiral geometrical elements that are essential for understanding their chiroptical activity: the molecular chirality of the adsorbed ligands and the atomic distortions of the underlying crystal lattice. The Asp and Pro surface ligands revealed different patterns of intermolecular bonding to the surface of the tungsten oxide that determines the position of chiroptical bands. The change from single (Pro) to double (Asp) C−O−W bridges between the amino acid and the $WO_{3-x}\cdot H_2O$ NPs resulted in the switch of the dominant chiroptical band from the green (Pro) to red (Asp) spectral region due to the change of the electronic transition primarily responsible for chiroptical activity. Subsequent efforts in this direction might include nuclear magnetic resonance (NMR) studies to elaborate on the distribution and dynamics of the surface ligands; further studies of magnetooptic phenomena may include the giant Zeeman splitting[124,125] and second-order magneto-chiral dichroism.[126,127]

The chemical significance of the chiral $WO_{3-x}\cdot H_2O$ NPs, and potentially other ceramic NPs, is asserted by catalysis of peptide-bond formation under mild conditions. Further studies in the direction of chiral catalysis[128] and photoinduced formation of peptide bonds in perspective of chirality transfer from photons to matter will be both fundamentally and technologically stimulating. Relevance of chiral ceramic NPs to optoelectronics,[129] photonics,[130] and biomedicine[63] is also envisioned.

ASSOCIATED CONTENT

Supporting Information

The Supporting Information is available free of charge on the ACS Publications website at DOI: 10.1021/jacs.7b01445.

Synthesis catalytic section, and characterization methods, MD simulations, calculations and relative figures (PDF)

AUTHOR INFORMATION

Corresponding Author

*kotov@umich.edu

ORCID

Zhi-Bei Qu: 0000-0003-1517-0822

Hilmi Volkan Demir: 0000-0003-1793-112X

Nicholas A. Kotov: 0000-0002-6864-5804

Notes

The authors declare no competing financial interest.

ACKNOWLEDGMENTS

The central part of this work was supported by the NSF projects "Ceramic Quasicrystals" NSF 1411014 and "Energy- and Cost-Efficient Manufacturing Employing Nanoparticles" NSF 1463474. Partial support of this work was also provided by the Center for Photonic and Multiscale Nanomaterials (C-PHOM) funded by the National Science Foundation (NSF) Materials Research Science and Engineering Center program DMR 1120923 as well as NSF projects 1403777. The authors thank Prof. Luis Liz-Marzan from CIC BiomaGUNE, Prof. Alexander Govorov from Ohio University and Prof. Mikhail Noginov from

DOI: 10.1021/jacs.7b01445
J. Am. Chem. Soc. 2017, 139, 13701−13712

Norfolk State University for helpful discussions. The authors are grateful to the University of Michigan's Electron Microscopy and Analysis Laboratory (EMAL) for assistance with XPS and electron microscopy. S.J. thanks the China Scholarship Council and Tianjin University for scholarships and support. M.C. acknowledges the support of the Swiss National Science Foundation Early Postdoc Mobility Fellowship (grant no. P2GEP2-165061).

REFERENCES

(1) Gallagher, S. a.; Moloney, M. P.; Wojdyla, M.; Quinn, S. J.; Kelly, J. M.; Gun'ko, Y. K. *J. Mater. Chem.* **2010**, *20*, 8350.
(2) Xia, Y.; Zhou, Y.; Tang, Z. *Nanoscale* **2011**, *3*, 1374.
(3) Yan, W.; Xu, L.; Xu, C.; Ma, W.; Kuang, H.; Wang, L.; Kotov, N. A. *J. Am. Chem. Soc.* **2012**, *134*, 15114.
(4) Valev, V. K.; Baumberg, J. J.; Sibilia, C.; Verbiest, T. *Adv. Mater.* **2013**, *25*, 2517.
(5) Ben-Moshe, A.; Maoz, B. M.; Govorov, A. O.; Markovich, G. *Chem. Soc. Rev.* **2013**, *42*, 7028.
(6) Yeom, J.; Yeom, B.; Chan, H.; Smith, K. W.; Dominguez-Medina, S.; Bahng, J. H.; Zhao, G.; Chang, W.-S.; Chang, S.-J.; Chuvilin, A.; Melnikau, D.; Rogach, A. L.; Zhang, P.; Link, S.; Král, P.; Kotov, N. A. *Nat. Mater.* **2015**, *14*, 66.
(7) Kim, Y.; Yeom, B.; Arteaga, O.; Yoo, S. J.; Lee, S.-G.; Kim, J.-G.; Kotov, N. A. *Nat. Mater.* **2016**, *15*, 461.
(8) Kotov, N. A. *Science* **2010**, *330*, 188.
(9) Yasukawa, T.; Miyamura, H.; Kobayashi, S. *Chem. Soc. Rev.* **2014**, *43*, 1450.
(10) Yasukawa, T.; Suzuki, A.; Miyamura, H.; Nishino, K.; Kobayashi, S. *J. Am. Chem. Soc.* **2015**, *137*, 6616.
(11) Gansel, J. K.; Thiel, M.; Rill, M. S.; Decker, M.; Bade, K.; Saile, V.; von Freymann, G.; Linden, S.; Wegener, M. *Science* **2009**, *325*, 1513.
(12) Wu, X.; Xu, L.; Liu, L.; Ma, W.; Yin, H.; Kuang, H.; Wang, L.; Xu, C.; Kotov, N. A. *J. Am. Chem. Soc.* **2013**, *135*, 18629.
(13) Hentschel, M.; Schäferling, M.; Weiss, T.; Liu, N.; Giessen, H. *Nano Lett.* **2012**, *12*, 2542.
(14) Ma, W.; Kuang, H.; Xu, L.; Ding, L.; Xu, C.; Wang, L.; Kotov, N. A. *Nat. Commun.* **2013**, *4*, 2689.
(15) Tamura, M.; Fujihara, H. *J. Am. Chem. Soc.* **2003**, *125*, 15742.
(16) Schaaff, T. G.; Whetten, R. L. *J. Phys. Chem. B* **2000**, *104*, 2630.
(17) Shemer, G.; Krichevski, O.; Markovich, G.; Molotsky, T.; Lubitz, I.; Kotlyar, A. B. *J. Am. Chem. Soc.* **2006**, *128*, 11006.
(18) Zhou, Y.; Yang, M.; Sun, K.; Tang, Z.; Kotov, N. A. *J. Am. Chem. Soc.* **2010**, *132*, 6006.
(19) Elliott, S. D.; Moloney, M. P.; Gun'ko, Y. K. *Nano Lett.* **2008**, *8*, 2452.
(20) Ma, W.; Xu, L.; de Moura, A. F.; Wu, X.; Kuang, H.; Xu, C.; Kotov, N. A. *Chem. Rev.* **2017**, *117*, 8041.
(21) Li, H. B.; Page, A. J.; Irle, S.; Morokuma, K. *J. Am. Chem. Soc.* **2012**, *134*, 15887.
(22) Vercosa, D. G.; Barros, E. B.; Souza Filho, A. G.; Mendes Filho, J.; Samsonidze, G. G.; Saito, R.; Dresselhaus, M. S. *Phys. Rev. B: Condens. Matter Mater. Phys.* **2010**, *81*, 165430.
(23) Liu, H.; Nishide, D.; Tanaka, T.; Kataura, H. *Nat. Commun.* **2011**, *2*, 309.
(24) Tu, X.; Manohar, S.; Jagota, A.; Zheng, M. *Nature* **2009**, *460*, 250.
(25) Mustonen, K.; Laiho, P.; Kaskela, A.; Zhu, Z.; Reynaud, O.; Houbenov, N.; Tian, Y.; Susi, T.; Jiang, H.; Nasibulin, A. G.; Kauppinen, E. I. *Appl. Phys. Lett.* **2015**, *107*, 013106.
(26) Suzuki, N.; Wang, Y.; Elvati, P.; Qu, Z.-B.; Kim, K.; Jiang, S.; Baumeister, E.; Lee, J.; Yeom, B.; Bahng, J. H.; Lee, J.; Violi, A.; Kotov, N. A. *ACS Nano* **2016**, *10*, 1744.
(27) George, J.; George Thomas, K. *J. Am. Chem. Soc.* **2010**, *132*, 2502.
(28) Slocik, J. M.; Govorov, A. O.; Naik, R. R. *Nano Lett.* **2011**, *11*, 701.
(29) Morrow, S. M.; Bissette, A. J.; Fletcher, S. P. *Nat. Nanotechnol.* **2017**, *12*, 410.
(30) Mukhina, M. V.; Maslov, V. G.; Baranov, A. V.; Fedorov, A. V.; Orlova, A. O.; Purcell-Milton, F.; Govan, J.; Gun'ko, Y. K. *Nano Lett.* **2015**, *15*, 2844.
(31) Baimuratov, A. S.; Gun'ko, Y. K.; Baranov, A. V.; Fedorov, A. V.; Rukhlenko, I. D. *Sci. Rep.* **2016**, *6*, 23321.
(32) Castro, D. T.; Ying, J. Y. *Nanostruct. Mater.* **1997**, *9*, 67.
(33) Arie, T.; Akita, S.; Nakayama, Y. *J. Phys. D: Appl. Phys.* **1998**, *31*, L49.
(34) Paul, W.; Sharma, C. P. *Am. J. Biochem. Biotechnol.* **2006**, *2*, 41.
(35) Vallet-Regí, M.; Ruiz-Hernández, E. *Adv. Mater.* **2011**, *23*, 5177.
(36) Tang, Z.; Kotov, N. A.; Magonov, S.; Ozturk, B. *Nat. Mater.* **2003**, *2*, 413.
(37) Orgel, L. E. *Trends Biochem. Sci.* **1998**, *23*, 491.
(38) Adachi, K.; Tanaka, S.; Yamazaki, S.; Takechi, H.; Tsukahara, S.; Watarai, H. *New J. Chem.* **2012**, *36*, 2167.
(39) Govan, J.; Gun'ko, Y. K. *Nanoscience* **2016**, *3*, 1.
(40) Seisenbaeva, G. A.; Moloney, M.; Tekoriute, R.; Hardy-Dessources, A.; Nedelec, J.-M.; Gun'ko, Y. K.; Kessler, V. G. *Langmuir* **2010**, *26*, 9809.
(41) Wang, B.; Chi, C.; Shan, W.; Zhang, Y.; Ren, N.; Yang, W.; Tang, Y. *Angew. Chem., Int. Ed.* **2006**, *45*, 2088.
(42) Liu, W.; Zhu, Z.; Deng, K.; Li, Z.; Zhou, Y.; Qiu, H.; Gao, Y.; Che, S.; Tang, Z. *J. Am. Chem. Soc.* **2013**, *135*, 9659.
(43) Lambert, J. F. *Origins Life Evol. Biospheres* **2008**, *38*, 211.
(44) Zamaraev, K.; Romannikov, V.; Salganik, R.; Wlassoff, W.; Khramtsov, V. *Origins Life Evol. Biospheres* **1997**, *27*, 325.
(45) Sebben, D.; Pendleton, P. *J. Chem. Thermodyn.* **2015**, *87*, 96.
(46) Lahav, N.; White, D. H. *J. Mol. Evol.* **1980**, *16*, 11.
(47) Rao, M.; Odom, D. G.; Oró, J. *J. Mol. Evol.* **1980**, *15*, 317.
(48) Lahav, N.; White, D.; Chang, S. *Science* **1978**, *201*, 67.
(49) Brack, A. *Dev. Clay Sci.* **2006**, *1*, 379.
(50) Ponnamperuma, C.; Shimoyama, A.; Friebele, E. *Origins Life* **1982**, *12*, 9.
(51) Rodriguez-Garcia, M.; Surman, A. J.; Cooper, G. J. T.; Suárez-Marina, I.; Hosni, Z.; Lee, M. P.; Cronin, L. *Nat. Commun.* **2015**, *6*, 8385.
(52) Bondy, S. C.; Harrington, M. E. *Science* **1979**, *203*, 1243.
(53) Jackson, T. A. *Science* **1979**, *206*, 483.
(54) Bonner, W. A.; Kavasmaneck, P. R.; Martin, F. S.; Flores, J. J. *Science* **1974**, *186*, 143.
(55) Thompson, T. D. *Clays Clay Miner.* **1973**, *21*, 351.
(56) Flores, J. J.; Bonner, W. A. *J. Mol. Evol.* **1974**, *3*, 49.
(57) McCullough, J. J.; Lemmon, R. M. *J. Mol. Evol.* **1974**, *3*, 57.
(58) Schreiner, E.; Nair, N. N.; Wittekindt, C.; Marx, D. *J. Am. Chem. Soc.* **2011**, *133*, 8216.
(59) Chen, Z.; Wang, Q.; Wang, H.; Zhang, L.; Song, G.; Song, L.; Hu, J.; Wang, H.; Liu, J.; Zhu, M.; Zhao, D. *Adv. Mater.* **2013**, *25*, 2095.
(60) Manthiram, K.; Alivisatos, A. P. *J. Am. Chem. Soc.* **2012**, *134*, 3995.
(61) Hollinger, G.; Minh Duc, T.; Deneuville, A. *Phys. Rev. Lett.* **1976**, *37*, 1564.
(62) Lou, Z.; Gu, Q.; Xu, L.; Liao, Y.; Xue, C. *Chem. - Asian J.* **2015**, *10*, 1291.
(63) Zhou, Z.; Kong, B.; Yu, C.; Shi, X.; Wang, M.; Liu, W.; Sun, Y.; Zhang, Y.; Yang, H.; Yang, S. *Sci. Rep.* **2015**, *4*, 3653.
(64) Berggren, L.; Azens, A.; Niklasson, G. A. *J. Appl. Phys.* **2001**, *90*, 1860.
(65) Saenger, M. F.; Höing, T.; Hofmann, T.; Schubert, M. *Phys. Status Solidi A* **2008**, *205*, 914.
(66) Saenger, M. F.; Höing, T.; Robertson, B. W.; Billa, R. B.; Hofmann, T.; Schubert, E.; Schubert, M. *Phys. Rev. B: Condens. Matter Mater. Phys.* **2008**, *78*, 245205.
(67) Schirmer, O.; Wittwer, V.; Baur, G.; Brandt, G. *J. Electrochem. Soc.* **1977**, *124*, 749.
(68) Moloney, M. P.; Gun'ko, Y. K.; Kelly, J. M. *Chem. Commun.* **2007**, *7345*, 3900.
(69) Gautier, C.; Bürgi, T. *J. Am. Chem. Soc.* **2008**, *130*, 7077.
(70) Feringa; van Delden, R. A. *Angew. Chem., Int. Ed.* **1999**, *38*, 3418.
(71) De Greef, F. A.; Smulders, M. J.; Wolffs, M.; Schenning, A. P. H. J.; Sijbesma, R. P.; Meijers, E. W. *Chem. Rev.* **2009**, *109*, 5687.
(72) Fasel, R.; Parschau, M.; Ernst, K.-H. *Nature* **2006**, *439*, 449.

DOI: 10.1021/jacs.7b01445
J. Am. Chem. Soc. 2017, 139, 13701−13712

(73) Szymanski, J. an; Roberts, A. C. *Can. Mineral.* **1984**, *22*, 681.
(74) Xie, F. Y.; Gong, L.; Liu, X.; Tao, Y. T.; Zhang, W. H.; Chen, S. H.; Meng, H.; Chen, J. *J. Electron Spectrosc. Relat. Phenom.* **2012**, *185*, 112.
(75) Corrêa, D. S.; Pazinato, J. C. O.; de Freitas, M. A.; Dorneles, L. S.; Radtke, C.; Garcia, I. T. S. *J. Braz. Chem. Soc.* **2014**, *25*, 822.
(76) Vasilopoulou, M.; Soultati, A.; Georgiadou, D. G.; Stergiopoulos, T.; Palilis, L. C.; Kennou, S.; Stathopoulos, N. a.; Davazoglou, D.; Argitis, P. *J. Mater. Chem. A* **2014**, *2*, 1738.
(77) Lu, D. Y.; Chen, J.; Zhou, J.; Deng, S. Z.; Xu, N. S.; Xu, J. B. *J. Raman Spectrosc.* **2007**, *38*, 176.
(78) Wagner, C.; Fournier, N.; Ruiz, V. G.; Li, C.; Müllen, K.; Rohlfing, M.; Tkatchenko, A.; Temirov, R.; Tautz, F. S. *Nat. Commun.* **2014**, *5*, 5568.
(79) Tang, Z.; Kotov, N. A.; Giersig, M. *Science* **2002**, *297*, 237.
(80) Stephens, P. J. *Annu. Rev. Phys. Chem.* **1974**, *25*, 201.
(81) Artemyev, M.; Krutokhvostov, R.; Melnikau, D.; Oleinikov, V.; Sukhanova, A.; Nabiev, I. Low-field magnetic circular dichroism in silver and gold colloidal nanoparticles of different sizes, shapes, and aggregation states. *Proceedings of SPIE*; Stockman, M. I., Ed.; SPIE: Bellingham, WA, 2012; Vol. *8457*, p 845729.
(82) Yao, H.; Shiratsu, T. *Nanoscale* **2016**, *8*, 11264.
(83) Hu, P.; Chen, L.; Kang, X.; Chen, S. *Acc. Chem. Res.* **2016**, *49*, 2251.
(84) Shoute, L. C. T.; Loppnow, G. R. *J. Am. Chem. Soc.* **2003**, *125*, 15636.
(85) Suri, K.; Annapoorni, S.; Sarkar, A. K.; Tandon, R. P. *Sens. Actuators, B* **2002**, *81*, 277.
(86) Patil, D.; Seo, Y. K.; Hwang, Y. K.; Chang, J. S.; Patil, P. *Sens. Actuators, B* **2008**, *132*, 116.
(87) Pandey, N. K.; Tiwari, K.; Roy, A.; Mishra, A.; Govindan, A. *Int. J. Appl. Ceram. Technol.* **2013**, *10*, 150.
(88) Bechinger, C.; Burdis, M. S.; Zhang, J.-G. *Solid State Commun.* **1997**, *101*, 753.
(89) Lai, W. H.; Su, Y. H.; Teoh, L. G.; Tsai, Y. T.; Hon, M. H. *Mater. Trans.* **2007**, *48*, 1575.
(90) Joseph, V.; Matschulat, A.; Polte, J.; Rolf, S.; Emmerling, F.; Kneipp, J. *J. Raman Spectrosc.* **2011**, *42*, 1736.
(91) Fu, S.; Chang, H.; Hsu, Y.; Lin, Y. *Proc. SPIE* **2014**, *9161*, 916108.
(92) Wang, A. X.; Kong, X. *Materials* **2015**, *8*, 3024.
(93) Cong, S.; Yuan, Y.; Chen, Z.; Hou, J.; Yang, M.; Su, Y.; Zhang, Y.; Li, L.; Li, Q.; Geng, F.; Zhao, Z. *Nat. Commun.* **2015**, *6*, 7800.
(94) Muravitskaya, A.; Rumyantseva, A.; Kostcheev, S.; Dzhagan, V.; Stroyuk, O.; Adam, P.-M. *Opt. Express* **2016**, *24*, A168.
(95) Jain, P. K.; Huang, X.; El-Sayed, I. H.; El-Sayed, M. a. *Acc. Chem. Res.* **2008**, *41*, 1578.
(96) Caldwell, J. W.; Applequist, J. *Biopolymers* **1984**, *23*, 1891.
(97) Hooker, T. M.; Bayley, P. M.; Radding, W.; Schellman, J. A. *Biopolymers* **1974**, *13*, 549.
(98) Kudryavtsev, K. V.; Ivantcova, P. M.; Muhle-Goll, C.; Churakov, A. V.; Sokolov, M. N.; Dyuba, A. V.; Arutyunyan, A. M.; Howard, J. A. K.; Yu, C.-C.; Guh, J.-H.; Zefirov, N. S.; Bräse, S. *Org. Lett.* **2015**, *17*, 6178.
(99) Tterlikkis, L.; Loxsom, F. M.; Rhodes, W. *Biopolymers* **1973**, *12*, 675.
(100) Thomasson, K. A.; Applequist, J. *Biopolymers* **1991**, *31*, 529.
(101) Deb, S. K. *Philos. Mag.* **1973**, *27*, 801.
(102) Bechinger, C.; Oefinger, G.; Herminghaus, S.; Leiderer, P. *J. Appl. Phys.* **1993**, *74*, 4527.
(103) Deepa, M.; Sharma, N.; Varshney, P.; Varma, S. P.; Agnihotry, S. A. *J. Mater. Sci.* **2000**, *35*, 5313.
(104) Heo, J.; Hwang, C.-S. *Nanomaterials* **2016**, *6*, 82.
(105) Mary, Y. S.; Ushakumari, L.; Harikumar, B.; Varghese, H. T.; Panicker, C. Y. *J. Iran. Chem. Soc.* **2009**, *6*, 138.
(106) Nakamoto, K. *Infrafed and Raman Spectra of Inorganic and Coordination Compounds*, 4th ed.; Wiley: New York, 1986.
(107) Qi, H.; Hegmann, T. *J. Am. Chem. Soc.* **2008**, *130*, 14201.
(108) Noguez, C.; Garzón, I. L. *Chem. Soc. Rev.* **2009**, *38*, 757.
(109) Lee, J.; Hernandez, P.; Lee, J.; Govorov, A. O.; Kotov, N. A. *Nat. Mater.* **2007**, *6*, 291.
(110) Knoppe, S.; Bürgi, T. *Acc. Chem. Res.* **2014**, *47*, 1318.
(111) Miyauchi, M.; Takashima, Y.; Yamaguchi, H.; Harada, A. *J. Am. Chem. Soc.* **2005**, *127*, 2984.
(112) Slocik, J. M.; Govorov, A. O.; Naik, R. R. *Nano Lett.* **2011**, *11*, 701.
(113) Chen, W.; Bian, A.; Agarwal, A.; Liu, L.; Shen, H.; Wang, L.; Xu, C.; Kotov, N. A. *Nano Lett.* **2009**, *9*, 2153.
(114) Nair, N. N.; Schreiner, E.; Marx, D. *J. Am. Chem. Soc.* **2006**, *128*, 13815.
(115) Hazen, R. M.; Sverjensky, D. A. *Cold Spring Harbor Perspect. Biol.* **2010**, *2*, a002162.
(116) Eustis, S.; El-Sayed, M. A. *Chem. Soc. Rev.* **2006**, *35*, 209.
(117) Shanker, U.; Bhushan, B.; Bhattacharjee, G.; Kamaluddin. *Origins Life Evol. Biospheres* **2012**, *42*, 31.
(118) Fosgerau, K.; Hoffmann, T. *Drug Discovery Today* **2015**, *20*, 122.
(119) Forsythe, J. G.; Yu, S.-S. S.; Mamajanov, I.; Grover, M. A.; Krishnamurthy, R.; Fernandez, F. M.; Hud, N. V.; Fernndez, F. M.; Hud, N. V. *Angew. Chem., Int. Ed.* **2015**, *54*, 9871.
(120) Leyton, P.; Zárate, R. A.; Fuentes, S.; Paipa, C.; Gómez-Jeria, J. S.; Leyton, Y. *BioSystems* **2011**, *104*, 118.
(121) Wu, J.; Zhang, Z.; Yu, X.; Pan, H.; Jiang, W.; Xu, X.; Tang, R. *Chin. Sci. Bull.* **2011**, *56*, 633.
(122) Leyton, P.; Saladino, R.; Crestini, C.; Campos-Vallette, M.; Paipa, C.; Berríos, A.; Fuentes, S.; Zárate, R. A. *Amino Acids* **2012**, *42*, 2079.
(123) López Navarrete, J. T.; Hernández, V.; Ramírez, F. J. *J. Mol. Struct.* **1995**, *348*, 249.
(124) Yu, J. H.; Liu, X.; Kweon, K. E.; Joo, J.; Park, J.; Ko, K.-T.; Lee, D. W.; Shen, S.; Tivakornsasithorn, K.; Son, J. S.; Park, J.-H.; Kim, Y.-W.; Hwang, G. S.; Dobrowolska, M.; Furdyna, J. K.; Hyeon, T. *Nat. Mater.* **2010**, *9*, 47.
(125) Norberg, N. S.; Gamelin, D. R. *J. Appl. Phys.* **2006**, *99*, 08M104.
(126) Yannopapas, V.; Vanakaras, A. G. *ACS Photonics* **2015**, *2*, 1030.
(127) Rikken, G. L. J. A.; Raupach, E. *Nature* **1997**, *390*, 493.
(128) Song, J.; Huang, Z. F.; Pan, L.; Zou, J. J.; Zhang, X.; Wang, L. *ACS Catal.* **2015**, *5*, 6594.
(129) Cong, S.; Geng, F.; Zhao, Z. *Adv. Mater.* **2016**, *28*, 10518.
(130) Kuai, S. L.; Bader, G.; Ashrit, P. V. *Appl. Phys. Lett.* **2005**, *86*, 221110.

DOI: 10.1021/jacs.7b01445
J. Am. Chem. Soc. 2017, 139, 13701−13712